Journal of Chromatography A 1676 (2022) 463251

Contents lists available at ScienceDirect

Journal of Chromatography A

journal homepage: www.elsevier.com/locate/chroma

Kinetic performance comparison of superficially porous, fully porous and monolithic reversed-phase columns by gradient kinetic plots for the separation of protein biopharmaceuticals

Simon Jaag[a], Chunmei Wen[a], Benjamin Peters[b], Michael Lämmerhofer[a,*]

[a] Pharmaceutical (Bio-)Analysis, Institute of Pharmaceutical Sciences, University of Tübingen, Auf der Morgenstelle 8, 72076 Tübingen, Germany
[b] Instrumental Analytics R&D, Merck KGaA, Frankfurter Str. 250, 64293 Darmstadt, Germany

ARTICLE INFO

Article history:
Received 8 March 2022
Revised 31 May 2022
Accepted 13 June 2022
Available online 14 June 2022

Keywords:
Gradient kinetic plots
Monolithic columns
Core shell particle
Fully porous particle
UHPLC

ABSTRACT

To find the best performing column for the analysis of protein-based biopharmaceuticals is a significant challenge as meanwhile numerous modern columns with distinct stationary phase morphologies are available for reversed-phase liquid chromatography. Especially when besides morphology also several other column factors are different, it is hard to decide about the best performing column *a priori*. To cope with this problem, in the present work 13 different reversed-phase columns dedicated for protein separations were systematically tested by the gradient kinetic plot method. A comprehensive comparison of columns with different morphologies (monolithic, fully porous and superficially porous particle columns), particle sizes and pore diameters as well as column length was performed. Specific consideration was also given to various monolithic columns which recently shifted a bit out of the prime focus in the scientific literature. The test proteins ranged from small proteins starting from 12 kDa, to medium sized proteins (antibody subunits obtained after IdeS-digestion and disulphide reduction) and an intact antibody. The small proteins cytochrome c, lysozyme and β-lactoglobulin could be analysed with similar performance by the best columns of all three column morphologies while for the antibody fragments specific fully porous and superficially porous particle columns were superior. A 450 Å 3,5 µm superficially porous particle column showed the best performance for the intact antibody while a 1.7 µm fully porous particle column with 300 Å showed equivalent performance to the best superficially porous column with thin shell and 400 Å pore size for proteins between 12 and 25 kDa. While the majority of the columns had C4 bonding chemistry, the silica monolith with C18 bonding and 300 Å mesopore size approximated the best performing particle columns and outperformed a C4 300 Å wide-pore monolith. The current work can support the preferred choice for the most suitable reversed-phase column for protein separations.

1. Introduction

Biopharmaceuticals are playing an increasingly important role in the pharmaceutical market. In the period from January 2015 to July 2018 there were 53 new drug approvals by the US FDA, 20 were from biological origin which makes around 38% [1]. Thereby, monoclonal antibodies (mAbs) account for 53% of all biopharmaceuticals [2]. Monoclonal antibodies are more challenging to analyse due to their higher molecular mass and molecular heterogeneity consisting of glycoforms, high and low molecular weight variants and post-translational modifications including charge variants [3]. Reversed-phase liquid chromatography (RP-LC) is one of the most important techniques for the analytical characterization of intact proteins and separates variants based on their hydrophobicity. RP-LC is inherently compatible with mass spectrometric (MS) detection which makes RP-LC-MS a powerful analytical platform. Unfortunately, RP-LC is a denaturing technique thus the proteins lose their native structure, yet this may be associated with improved chromatographic efficiencies. Depending on the kind of organic modifier, different selectivity can be obtained [4]. The recovery of the proteins can be increased strongly by using elevated temperature because this reduces the secondary interactions with the stationary phase [5,6]. Mobile phase additives affect the peak shape (tailing), peak width but also the ion suppression of MS

Abbreviations: UHPLC, Ultra-high performance liquid chromatography; SPP, Superficially porous particle; FPP, Fully porous particle; KPL, kinetic performance limit.

* Corresponding author at: Pharmaceutical (Bio-)Analysis, Institute of Pharmaceutical Sciences, University of Tübingen, Auf der Morgenstelle 8, 72076 Tübingen, Germany.
E-mail address: michael.laemmerhofer@uni-tuebingen.de (M. Lämmerhofer).

https://doi.org/10.1016/j.chroma.2022.463251
0021-9673/

detection [5,7]. While trifluoroacetic acid is a strong ion-pairing agent and provides sharp peaks, formic acid is better suitable for MS detection due to its lower ion-suppression effects. RP-LC for proteins has an on-off like retention behaviour (due to steep adsorption isotherms) as at low elution strength the protein is completely retained while above a certain percentage of organic modifier the protein is not retained any more at all [8,9]. This is the reason why RP-LC for proteins is only done in gradient elution mode. However, this makes the comparison of different columns more challenging.

Special attention should be paid to the selection of a suitable pore size which is large enough to enable unhindered diffusion and avoid partial or total pore exclusion [10]. On the other hand, as the pore size increases, the specific surface area decreases, resulting in a decrease in retention and sample capacity. Pore sizes from 300 to 1000 Å are typically recommended for protein separations [11,12]. C4 alkyl and phenyl phases are usually used as stationary phases, since C18 phases were thought to bear the risk of irreversible binding of proteins to the column surface due to their strong hydrophobicity. Newer publications state that the recovery is mostly affected by ligand density, surface coverage, flexibility of the ligand, carbon load, relative hydrophobicity and the degree of exposure of the surface silanols [13]. Secondary interactions with the stationary phase can have a strong, negative effect on the separation and should be minimized with end-capping of free silanol groups (silica-based columns) and the use of higher temperatures or adding ancillary solvents like 1-butanol [5,6].

The column technology plays a key role for protein separations especially considering the mass transfer kinetics [14]. Non-porous particles are the most favourable in terms of the intra-particle mass transfer resistance but have the lowest surface area and are usually not used for RP-LC but for ion-exchange chromatography. Fully porous particles (FPPs) show the highest intra particle mass transfer resistance as the entire particle is accessible for diffusion. Superficially porous particles (SPPs) consist of a solid core covered by a porous shell. Therefore, the diffusion paths are significantly reduced and so is the mass transfer resistance [12]. Monolithic columns do not consist of individual particles but of a continuous chromatographic bed. They have large macropores which enable a low back pressure even at high flow rates and they have smaller mesopores for the actual solute interaction [15,16]. The support type of protein columns can be either silica-based or based on organic polymers. One advantage of the organic polymer-based supports is the better stability at higher pH-values and high temperatures.

A convenient method to evaluate the performance of columns with different lengths, diameters, and stationary phase morphologies are kinetic plots [17–19]. They are well known for isocratic LC, but rarely employed for gradient elution which is the common situation in protein separations, as mentioned above. The evaluation of the column performance in gradient RP using the gradient kinetic plots was introduced by Broeckhoven et al. [20] and the concept was already applied to RP-LC of proteins by Fekete et al. [21]. The performance of some SPP and FPP columns for proteins has been compared by Wagner et al. and Bobály et al. [10,22]. Fekete et al. recently published on the usage of ultra-short columns for protein separations and investigated new stationary phases for widepore columns [4,8].

The current work extends on these prior reports and is devised as a comprehensive, systematic column comparison study applying the gradient kinetic plot concept for many popular protein RP columns for the first time. Different column technologies differing in the stationary phase morphology were evaluated for a total of 13 columns, including three monolithic, six SPP and four FPP columns. Three different sample mixtures were used for the evaluation consisting of (i) a protein mixture with small proteins (cytochrome c, β-lactoglobulin and lysozyme), (ii) antibody fragments obtained after IdeS-digestion and disulphide reduction and (iii) an intact antibody to cover a wide range of molecular mass. After some initial screening runs, conditions for an appropriate comparison based on the gradient kinetic plot were evaluated and later used for the column comparison. To the best of our knowledge, there was no such comprehensive study on the performance of protein columns from different column technologies and suppliers reported until now, and in particular specific focus is paid to monolithic columns for which the recent literature is relatively lean. The groups of Teutenberg and Eeltink also applied gradient kinetic plots and compared packed bed and monolithic columns in capillary or microbore column format [23–25]. The influence of the column technology, particle size and pore size is thoroughly discussed.

2. Experimental

2.1. Materials

Chromolith WP300 RP-4 (4.6 × 50 mm, C4-modified monolithic silica column), Chromolith WP300 RP-18 (2.0 × 100 mm), Chromolith HR RP-18e (2.0 × 100 mm, high resolution research sample, C18-modified), BIOshell 400 Å Protein C4 (2.1 × 50 mm, 3.4 µm), BIOshell IgG 1000 Å C4 (2.1 × 20 mm & 2.1 × 50 mm, 2.7 µm) columns were generously provided by Merck (Darmstadt, Germany). Aeris Widepore C4 200 Å (2.1 × 50 mm, 3.6 µm) was supplied by Phenomenex (Aschaffenburg, Germany). The AdvanceBio RP-mAb C4 (2.1 × 50 mm, 3.5 µm) column was purchased from Agilent (Waldbronn, Germany). The BioResolve RP mAb (2.1 × 50 mm, 2.7 µm) and the Acquity UPLC protein BEH C4 (2.1 × 50 mm, 1.7 µm) columns were purchased from Waters (Eschborn, Germany) and the MAbPac RP column (4.0 × 50 mm, 4 µm) from Thermo Scientific (Waltham, Ma, USA). The Solas C4 400 Å and 1000 Å (both 2.1 × 50 mm, 1.7 µm) were obtained from Glantreo (Cork, Ireland). The properties of the columns are summarized in Tables 1–3. NIST monoclonal antibody (NISTmAb) reference material (RM) 8671, a humanized IgG1κ monoclonal antibody formulated in histidine buffer, was purchased from the National Institute of Standards and Technologies (NIST, Gaithersburg, MD, USA). Acetic acid (≥ 99.8%) and sodium dihydrogen phosphate monohydrate were from Merck. Tris(2-carboxyethyl)phosphine (TCEP), sodium chloride, potassium chloride, and sodium hydroxide, lysozyme from chicken egg white, cytochrome c from equine heart, β-lactoglobulin B from bovine milk (≥90%) and bovine serum albumin (BSA), Protein LoBind Tubes 1.5 mL from Eppendorf were purchased from Sigma-Aldrich (Merck, Taufkirchen, Germany). Di-sodium hydrogen phosphate anhydrous and thiourea were purchased from Applichem (Darmstadt, Germany). FragIT (immobilized IdeS enzyme) was supplied by Genovis (Luden, Sweden). Ultrapure water was obtained from a Purelab Ultra purification system from Elga LabWater (Celle, Germany).

2.2. Instrumentation and software

The LC-instrument was from Agilent Technologies (Waldbronn, Germany). Agilent 1290 Infinity UHPLC system consisting of binary pump (G4220A), autosampler (G4226A), sample thermostat (G1130B), thermostated column compartment (G1316C) and diode array detector (DAD, G4212A). The instrument was equipped with an ultra-low dispersion kit and the extra-column volume and dwell volume was determined as 11.7 µL and 175 µL, respectively. Instrument control and data analysis were performed using OpenLab CDS 2.5.0.

Microsoft Excel 2019 (Redmond, WA, USA) and OriginPro 2021b (OriginLab, Northapton, MA, USA) were used for data processing.

Table 1
Properties of superficially porous particle (SPP) columns. d_p: particle diameter, L × I.D.: column length and internal diameter, d(core): diameter of the SPP, shell: shell thickness of the SPP, ΔP_{max}: maximum pressure limit of the column, T_{max}: maximum column temperature, C [%]: carbon load, K_v: column permeability, Φ: flow resistance.

Column	d_p [µm]	L × I.D. [mm]	pore size [Å]	d (core) [µm]	shell [µm]	ΔP_{max} [bar]	sup-port	station-ary phase	pH range	T_{max}. [°C]	C [%]	K_v [m²]	Φ[/]
AdvanceBio RP-mAb C4	3.5	50 × 2.1	450	3	0.25	600	silica	C4	1 to 8	90	n/a	$1.12*10^{-14}$	$1.10*10^{3}$
Aeris Widepore C4	3.6	50 × 2.1	200	3.2	0.2	600	silica	C4	1.5 to 9	90	n/a	$9.14*10^{-15}$	$1.42*10^{3}$
BioResolve RP mAb	2.7	50 × 2.1	450	1.9	0.4	689	silica	Phenyl	2 to 7.5	90	5.48	$8.08*10^{-15}$	$9.03*10^{2}$
BIOshell A400 Protein C4	3.4	50 × 2.1	400	3	0.2	600	silica	C4	2 to 9	60	0.4	$7.82*10^{-15}$	$1.48*10^{3}$
BIOshell IgG 1000A C4	2.7	50 × 2.1	1000	1.7	0.5	1000	silica	C4	2 to 9	60	0.6	$7.25*10^{-15}$	$1.01*10^{3}$
BIOshell IgG 1000A C4	2.7	20 × 2.1	1000	1.7	0.5	1000	silica	C4	2 to 9	60	0.6	$5.85*10^{-15}$	$1.25*10^{3}$

Table 2
Properties of fully porous particle columns. d_p: particle diameter, L × I.D.: column length and internal diameter, ΔP_{max}: maximum pressure limit of the column, T_{max}: maximum column temperature, C [%]: carbon load, K_v: column permeability, Φ: flow resistance.

Column	d_p [µm]	L × I.D. [mm]	pore size [Å]	ΔP_{max} [bar]	stationary phase	support	pH range	T_{max}. [°C]	C [%]	K_v [m²]	Φ[/]
Acquity UPLC Protein BEH C4	1.7	50 × 2.1	300	1000	C4	ethylene silica hybrid	1 to 12	90	7.95	$3.31*10^{-15}$	$8.74*10^{2}$
MAbPac RP	4	50 × 2.1	1500	275	Phenyl	DVB	0 to 14	110	n/a	$5.81*10^{-15}$	$2.75*10^{3}$
Solas C4 1000A	1.7	50 × 2.1	1000	700	C4	silica	2 to 9	90	0.33	$2.48*10^{-15}$	$1.16*10^{3}$
Solas, C4 400A	1.7	50 × 2.1	400	700	C4	silica	2 to 9	90	0.69	$2.29*10^{-15}$	$1.26*10^{3}$

Table 3
Properties of monolithic columns. L × I.D.: column length and internal diameter, ΔP_{max}: maximum pressure limit of the column, T_{max}: maximum column temperature, C [%]: carbon load.

Column	L × I.D. [mm]	Macropore size [µm] [a]	Meso-pore size [Å]	porosity	ΔP_{max} [bar]	pH range	T_{max}[°C]	Support	Stationary phase	C [%]
Chromolith WP300 RP-4	50 × 4.6	2	300	>80%	200	1.5 to 7.5	60	silica	C4	3.5
Chromolith WP300 RP-18	100 × 2	2.0	300	>80%	200	1.5 to 7.5	60	silica	C18	9
Chromolith HR RP-18e	100 × 2	1.15	150	>80%	200	2.0 to 7.5	50	silica	C18	15

[a] Values taken from Chromolith column brochure at https://www.sigmaaldrich.com/

DryLab 4.3.5 (Molnár-Institute, Berlin, Germany) as design of experiment software.

2.3. Sample preparation

A stock solution of the protein samples cytochrome c, β-lactoglobulin, lysozyme and BSA with a concentration of 5 mg/mL has been prepared with water. The stock solutions were diluted 1:5 with 10 mM ammonium acetate (pH 6) to get the final concentration of the pure proteins (c = 1 mg/mL). A mixture of the four proteins with a concentration of 1 mg/mL for each protein was prepared by mixing the four stock solutions and dilution by 10 mM ammonium acetate. NIST mAb was diluted from a concentration of 10 mg/mL to 1 mg/mL with 10 mM ammonium acetate.

IdeS digestion was performed with FragIT MicroSpin columns following the manufacturer's instructions with a cleavage buffer composed of 10 mM Na_2HPO_4, 140 mM NaCl and 2.7 mM KCl. 20 µL of the antibody solution (c = 10 mg/mL) was diluted with 80 µL cleavage buffer. For digestion this reaction mixture was incubated for 30 min at 37 °C and 250 rpm. For further reduction, 20 µL of a 50 mM TCEP solution was added and incubated for 60 min at 60 °C and 250 rpm. Subsequently, the buffer was exchanged three times with a Vivaspin 500 spin column (MWCO 10,000) with 10 mM ammonium acetate buffer pH 6.0 at 12 000 g for 5 min.

2.4. Gradient kinetic plot method

The gradient kinetic plots concept has been described by Broeckhoven et al. [20] and the same methodology was used herein with some minor adjustments. In pre-experiments the column dead times and the system back pressure were measured isocratically by injection of thiourea as dead time marker with the mobile phase composition with the highest viscosity during the gradient which is for an acetonitrile/water mixture at 25% for the gradient ranges from 25–50% ACN [26]. The back pressure was measured with the column installed (ΔP_{total}) and with a zero-dead volume union installed instead of the column (ΔP_{ec}). Thus, the corrected column back pressure (ΔP_{column}) could be calculated by $\Delta P_{column} = \Delta P_{total} - \Delta P_{ec}$. The maximum flow rate was determined according to the maximum allowed column pressure given by the manufacturer. Eight data points representing eight different flow rates were considered as sufficient for creation of the gradient kinetic plots. The highest flow rate was dictated by the maximum allowed column pressure $\Delta P_{column,\ max}$ thus the remaining seven flow rates were selected considering the lowest flow rate with sufficient flow accuracy specified by the instrument manufacturer (0.1 mL/min) and the remaining six flow rates were in equal intervals in between. DryLab screening runs were performed for each column to check for appropriate conditions considering the column temperature and the gradient design (start and end condition of acetonitrile and gradient time). Three different gradient times (10, 20 and 30 min) were used at two different temperatures (30 and 60 °C) at a flow rate of 0.5 mL/min for the screening and determination of log k_w and S-values, thus in total six gradient runs were performed. For the DryLab model only the 10 and 30 min runs were used as input and the 20 min gradient time was used to determine the method and sample dependent S-value according to a method described by Zhang et al. [27] with some adjustments explained in the supplementary chapter 1. Based on the linear solvent strength theory the log k_w and S-values can be calculated as intercept and slope, respectively, of $log\ k$ vs. φ plots (φ: modifier content).

For each column the lowest possible gradient time was used to get still a separation of all peaks with a minimal resolution of 1.5. As the intact NISTmAb samples has only one peak the low-

est possible gradient time was used and the retention time of the NISTmAb peak was set to 2/3 of the gradient time.

One important prerequisite for the gradient kinetic plots is that for each flow rate the sample experienced the same mobile phase history [20]. Therefore, $\beta \cdot t_0$ must be constant, where β is the gradient steepness and t_0 is the column dead time.

The gradient steepness β can be expressed as [20] (Eq. (1))

$$\beta = \frac{\varphi_{end} - \varphi_0}{t_{end} - t_{start}} = \frac{\Delta\varphi}{t_G} \quad (1)$$

Where t_{end} and t_{start} are the gradient end and start time and φ_{end} and φ_0 are the final and initial organic modifier percentage, respectively.

In the current study, columns with different stationary phases were used why it might not be enough to keep $\beta \cdot t_0$ constant. Zhang et al. suggested to consider the *S*-value and keep $S \cdot \beta \cdot t_0$ constant.

The comparison of the chromatographic performance of the different columns in gradient separations was performed using the peak capacity (n_p). The peak capacity represents the maximum number of peaks that can be fitted into the chromatographic window between the first and the last eluting peak. Herein, n_p was calculated assuming $Rs = 1$ using a simplified equation [28]:

$$n_p = 1 + \frac{t_G - t_0}{W_{4\sigma}} = 1 + \frac{t_G - t_0}{1.7 \cdot W_{50\%}} \quad (2)$$

with t_0 being the elution time of a non-retained compound (dead time) and t_G being the gradient (run) time. $w_{4\sigma}$ is the peak width at 4σ and $w_{50\%}$ is the peak width at half height. $w_{50\%}$ was used because it can be determined more accurately by the software and is less prone to errors.

The maximum column performance limit is reached at its kinetic performance limit (KPL) which is at the maximum pressure limit (ΔP_{max}) either of the column or the system, whichever is the lower. Therefore, the column length rescaling factor λ was used to calculate the peak capacity at the KPL [20].

$$\lambda = \frac{\Delta P_{max}}{\Delta P_{exp}} \quad (3)$$

Where ΔP_{exp} is the experimental pressure drop caused by the column.

The peak capacity at the KPL can be calculated as follows based on the experimentally obtained peak capacity $n_{p,exp}$:

$$n_{p,KPL} = 1 + \sqrt{\lambda} \cdot (n_{p,exp} - 1) \quad (4)$$

The retention time at the KPL limit can be calculated as follows:

$$t_{R,KPL} = \lambda \cdot t_{R,exp} = t_{0,\,KPL}(1 + k) \quad (5)$$

In the final KPL methods the gradient range was from 25 – 55% ACN and a column temperature of 60 °C was used for all columns.

3. Results and discussion

3.1. Validation of the gradient kinetic plot concept for proteins

First, the validity of the gradient kinetic plot model for proteins as solutes was investigated using two columns which only differed in their column length viz. BIOshell 1000 Å 50 mm and 20 mm length. For this reason, the KPL curves of the two columns should overlap proving the validity of the model [20]. The sample set consisted of proteins covering a molecular weight range from 12.4 to 148.2 kDa, isoelectric points (*pI*) ranging from 4.7 to 11.35 and different hydrophobicities (Table S 1). Three sample mixtures were used: A standard protein mixture consisting of cytochrome c, lysozyme and β-lactoglobulin covers the molecular weight range from 12.4 to 18.3 kDa representing small proteins (note, BSA was also present and hence appears in the chromatograms; however, due to molecular dispersity and uncommonly broad peaks it was omitted from the study of KPL curves). Antibody fragments obtained after IdeS-digestion and disulphide reduction resulting in light chain (LC), Fc/2- and Fd-fragments are frequently analysed in middle-up approaches and represent intermediate-sized proteins with a molecular weight of approximately 25 kDa. The intact NISTmAb sample was the protein with the highest molecular weight in the study sample set.

Based on the DryLab screening runs similar conditions for the gradient range and the start and end percentage of acetonitrile (25 – 55%) as well as a temperature of 60 °C were found to be appropriate for all columns. The use of higher temperatures than 60 °C for columns with a higher maximum temperature limit will certainly have an influence on the column performance as it is affecting the selectivity, S-value of the solutes, on-column protein stability, the mobile phase viscosity and consequently the back pressure and therefore the maximum possible flow rate. Due to the multiple parallel effects of the temperature on the separation, it would be difficult to deconvolute the stationary phase effects responsible for the differences in column performance. Therefore, a fixed temperature of 60 °C was used for all columns as a compromise. Two different conditions have been tested for an overlap. First $\beta \cdot t_0$ was kept constant and a value of 0.02 was selected based on the screening runs. This approach is the original method from Broeckhoven et al. testing columns with the same stationary phase. Second $S \cdot \beta \cdot t_0$ was set constant as suggested by Zhang et al. [27] which takes the different retention behaviour of varying stationary phases for the same analyte into account. $S \cdot \beta \cdot t_0 = 2$ was found to be considerable based on the DryLab screening runs. For the first case with $\beta \cdot t_0 = 0.02$, a very good overlap could be observed for lysozyme (Fig. 1a), the antibody fragments (Fig. 1c) and the intact NISTmAb (Fig. 1e). Minor deviations were found for cytochrome c and β-lactogobulin (Fig. 1a). The overlap for the second condition $S \cdot \beta \cdot t_0 = 2$ was perfect for all sample proteins (Fig. 1b, d) with exception for the intact NISTmAb (Fig. 1f) which showed a minor deviation. Both tested conditions showed acceptable results but in total the condition $S \cdot \beta \cdot t_0 = 2$ seemed to be superior because only the NISTmAb showed a minor deviation and this might result from inaccurate determination of the *S*-value of the antibody.

3.2. Evaluation of superficially porous particle columns

The current study included six superficially porous particle (SPP) columns which differed mainly in shell thickness and pore size, while they had nearly the same particle diameter (2.7—3.5 µm) (Table 1). Example chromatograms for SPP columns (AdvanceBio RP mAb C4 and BIOshell 400 Å, respectively) are given in Fig. 2a-c and Fig. S 1 in the supplementary material for the intact NISTmAb, the NIST-IdeS-TCEP sample and the protein mixture. All main peaks of the NISTmAb fragments (Fig. 2b) as well as the protein mix samples (Fig. 2c) were baseline separated from each other.

The interpretation of the KPL curves is straightforward. From a practical viewpoint KPL plots of distinct columns can be conveniently used to select the system which can provide a certain efficiency (i.e. peak capacity n_p) in the shortest possible time t_R when they are operated at their pressure maximum ΔP_{max} (see Table 1). Vice versa, it allows to select the system that gives the highest peak capacity with a certain pre-selected speed t_R. For example, when looking at the KPL curves of different SPP columns for cytochrome c (Fig. 3a), $n_p = 100$ can be achieved in the shortest possible time with the BIOshell 400 Å column ($t_R = 55.9$ s, other columns: BIOshell 1000 Å 20 mm: 67.8 s; BioResolve RP mAb: 78.5 s; BIOshell 1000 Å 50 mm: 84.7 s; Advance Bio 89.6 s; Aeris Widepore C4: 94.3 s). The shortest analysis time for $n_p = 250$,

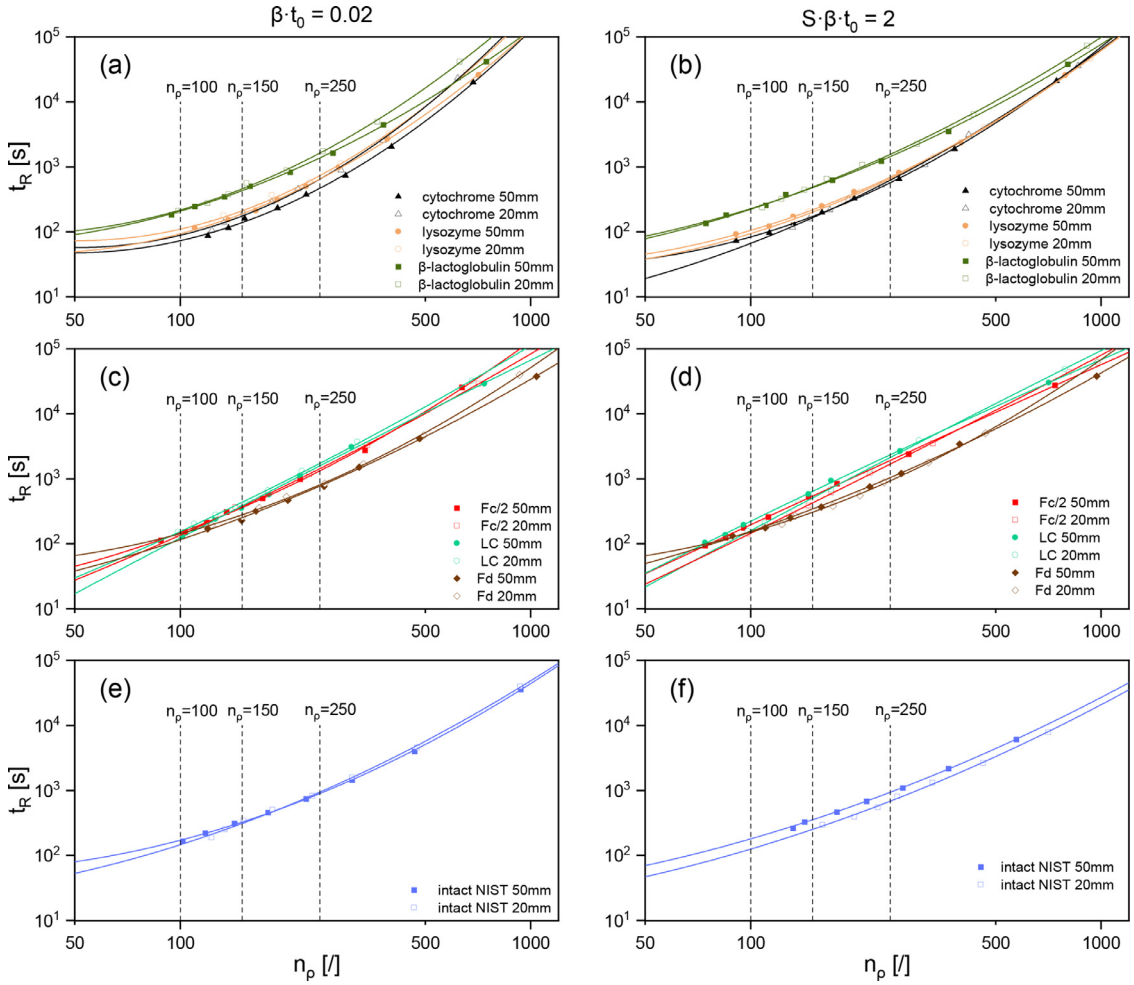

Fig. 1. Gradient kinetic plot method validation for protein samples using columns of different lengths. Protein mix sample (a-b) contained cytochrome c, lysozyme and β-lactoglobulin, (c-d) NISTmAb subunits comprised of Fc/2-, Fd-fragments and light chain (LC), and (e-f) intact NISTmAb. Columns: BIOshell 1000 Å 2.1 mm I.D., 50 and 20 mm length, respectively; column temperature = 60 °C; 8 flow rates from 0.1 to 1.5 in 0.2 mL/min steps; mobile phase A: 0.1% (v/v) TFA in water, B: 0.1% (v/v) TFA in ACN, gradient: 25–55% B; gradient time set to keep $\beta \cdot t_0 = 0.02$ (a, c, e) or $S \cdot \beta \cdot t_0 = 2$ (b, d, f) constant.

however, was observed for the BIOshell 1000 Å 50 mm column (t_R = 565.2 s). In general, the BIOshell 400 Å column showed superior performance especially for the fast method regime (low retention times; slant horizontal asymptote; C-term region) compared to the other SPP columns for the small proteins cytochrome c, lysozyme and β-lactoglobulin (Fig. 3a-c). At low flow rates and slow method regime (i.e. under conditions corresponding to the vertical asymptote; B-term region) the highest peak capacities were reached with the BIOshell 1000 Å columns. A similar trend was found for the lysozyme and β-lactoglobulin samples (Fig. 3b-c). These data suggest that the benefit of enhanced pore diffusion with 1000 Å material cannot be realized under conditions of high flow rates (fast separation regime; C-term region) due to the longer diffusion paths (0.5 µm shell thickness) of the BIOshell 1000 Å compared to BIOshell 400 Å (0.2 µm). Even for small proteins shorter diffusion paths (thin shell) bring more benefits at high flow rates than wider pores, the advantage in terms of unhindered pore diffusion can only be exploited at low flow rates if the diffusion paths are relatively long like for thick-shell SPP columns (such as BIOshell 1000 Å).

For intermediate-sized proteins, such as NISTmAb fragments, the BIOshell 400 Å column had the best performance amongst the tested SPP columns over the entire flow rate/column length range (Fig. 3d-f). Again, the outstanding performance of the BIOshell 400 Å column was most likely mainly due to the thinner porous shell (0.2 µm) with its shorter diffusion paths and enhanced mass transfer also for intermediate-size proteins. The larger the protein, the smaller is the diffusion coefficient and the higher is the mass transfer contribution to the band broadening. Thus, a better performance of the BIOshell 1000 Å was expected but was not realized, probably due to a more favourable striking effect from shorter diffusion paths of the BIOshell 400 Å material (Fig. 3d-f). The Aeris Widepore C4 column has the same shell thickness, but a much smaller pore size of 200 Å which seems to be too narrow and can lead to hindered pore diffusion. Therefore, it is not a surprise that it showed the worst performance of all SPP columns tested.

While the BIOshell 400 Å column was the best choice for proteins with a molecular weight from 12.4 to about 25 kDa, the AdvanceBio RP mAb C4 was superior to the other SPP columns for the intact NIST mAb (Fig. 3g). Without more in-depth characterizations and investigations of individual peak dispersion contributions it is hard to explain why it was superior to the BIOshell 400 Å column as they largely resemble each other in shell thickness (0.25 vs. 0.2 µm), particle size (3.5 vs. 3.4 µm) and pore size (450 vs. 400 Å). The permeability of the BIOshell 400 Å is 30 % lower while the flow resistance is 35 % higher compared to the AdvanceBio column which may indicate some significant differences in the morphology (see supplementary chapter 2.3 and Fig. S 2–3). Possible explanations for the shifted KPL curve of AdvanceBio RP mAb C4 in relation to the BIOshell 400 Å are differences in surface chem-

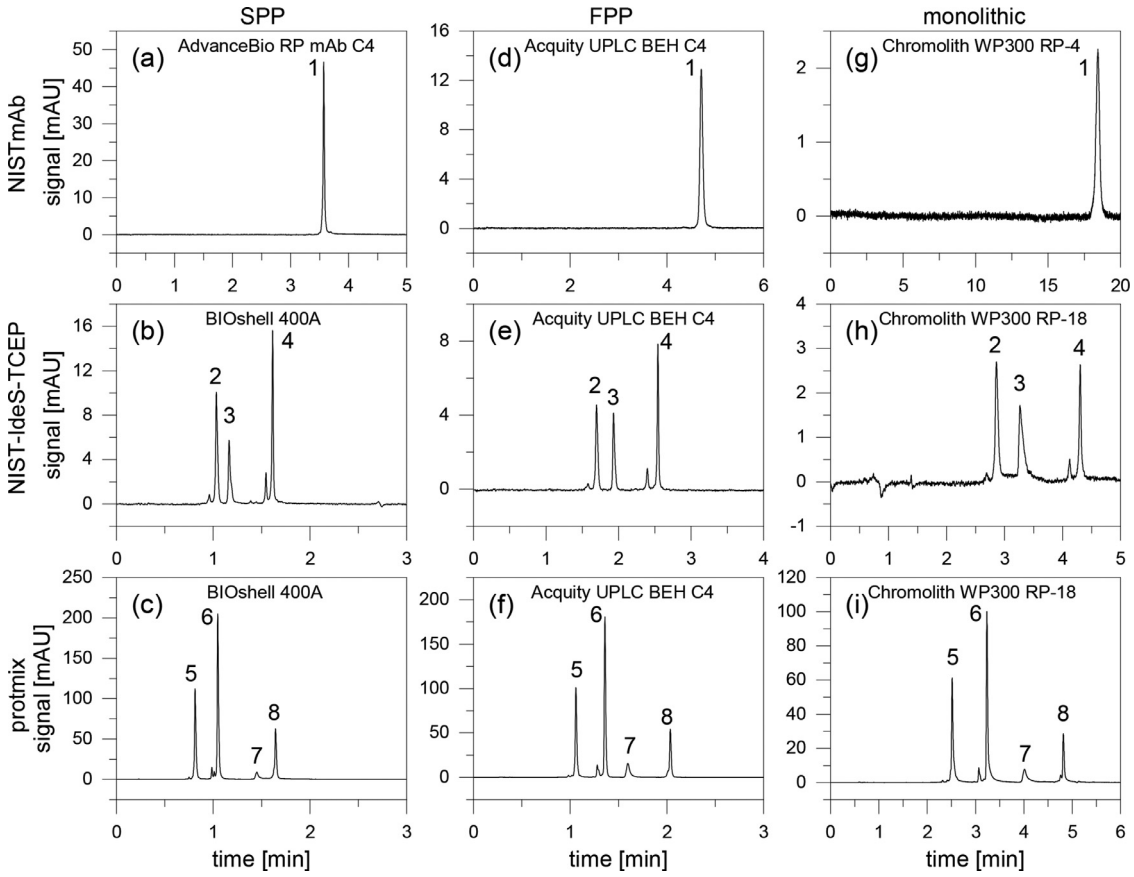

Fig. 2. Chromatograms of the best performing columns for each column technology. Superficially porous particle (SPP) columns (a, d, g); fully porous particle (FPP) columns (b, e, h); monolithic columns (c, f, i) Samples: intact NISTmAb (a-c), NISTmAb fragments (NIST-IdeS-TCEP: d-f) and protein mixture (g-i). Column temperature = 60 °C, flow rate = 0.5 mL/min, mobile phase A: 0.1% (v/v) TFA in water, B: 0.1% (v/v) TFA in ACN, gradient 25–55% B. Gradient time was set for each column and sample mixture to keep $S{\cdot}\beta{\cdot}t0 = 2$.

istry including bonding density, endcapping and secondary interactions of the stationary phase, pore structure, pore and particle diameter distributions, and so forth. The suitability of the BIOshell columns for ultra-fast protein separations (<1.5 min) has been recently demonstrated by their application for full comprehensive 2D-LC analysis [29].

For comparison of the KPL curves of different proteins on the same SPP column, the interested reader is referred to the supplementary material (Fig. S 4). To conclude, the relative order of kinetic performance of the tested SPP columns is mainly driven by the shell thickness, unless the pore diameter is too small like for the 200 Å material. A significant gain in the kinetic performance with 1000 Å pore size can only be materialized in the slow method regime (due to thicker shell). To investigate the influence of the pressure limit on the performance comparison, a KPL plot with a constant maximum pressure (600 bar) limit was created (see supplementary Fig. S 5) but still the same trends were observed without any significant changes. The current work confirms that the 400 Å materials with thin 0.2 µm shell are a good compromise regarding kinetic performance.

3.3. Evaluation of fully porous particle columns

Four different fully porous particle (FPP) columns have been investigated in the current study differing in particle size (1.7 and 4 µm), pore size (300 to 1500 Å) and backbone chemistry (silica, ethylene bridged silica hybrid, polystyrene materials) (Table 2). In the direct column-to-column comparison the Acquity UHPLC BEH C4 (1.7 µm, 300 Å) column outperformed clearly all other FPP columns among all the examined proteins and the entire tested flow rate range (Fig. 4). The difference in performance between the Acquity and the Solas columns could be partially explained by the lower maximum pressure limit of the Solas columns (700 bar vs. 1000 bar). As a consequence, the Solas columns allowed the use of lower maximum flow rates up to 0.8 mL/min only, while the Acquity column could be run at up to 1.5 mL/min. Therefore, faster protein analysis can be realized with the Acquity column. The Solas columns possess also a low carbon content (Table 2). One could further speculate that due to low ligand coverage residual silanols are accessible to protein interactions at the surface leading to reduced efficiencies. On the other hand, the wide-pore (1500 Å) 4 µm MAbPac RP column was performing worst for the small proteins in terms of speed-efficiency compromise and kinetic performance limits, respectively, under the selected conditions (60 °C) most likely owing to its larger particle size that is associated with larger Eddy diffusion terms and increased mass transfer resistance (Fig. 4). Here it should be mentioned that MAbPac RP is usually used at higher temperatures at which it shows significantly better performance. As the size of the proteins increased, the MAbPac RP column gained in KPL performance and indeed its best KPL-curves amongst the tested proteins were obtained for the intact NISTmAb and its fragments (Fig. S 6a). This observation can be explained by the large pore size of 1500 Å which is specifically appropriate for very large proteins. For the Acquity UPLC BEH C4 column the KPL curves show less variance between the distinct proteins but again the NISTmAb sample and the Fd-fragment exhibited the best KPL-curves (Fig. S 6b). One further advantage of the Acquity column may be the broader pH range from pH 1 to 12 due to the bridged

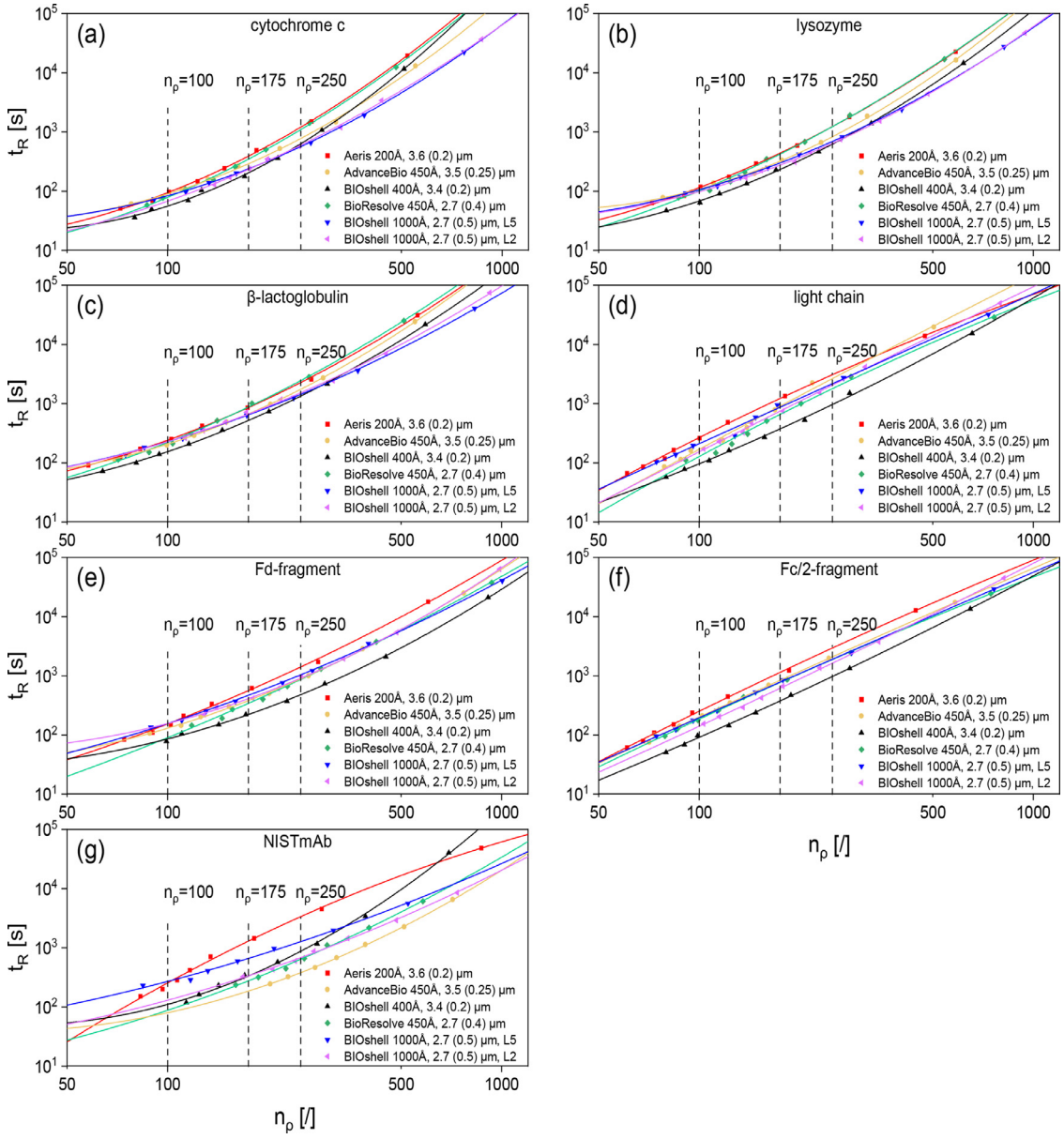

Fig. 3. Gradient kinetic plots for the same protein and different superficially porous particle columns. (a) Cytochrome c, (b) lysozyme, (c) β-lactoglobulin, (d) light chain, (e) Fd-fragment, (f) Fc/2-fragment, (g) NIST mAb. Column temperature = 60 °C, mobile phase A: 0.1% (v/v) TFA in water, B: 0.1% (v/v) TFA in ACN; gradient: 25–55% B; 8 flow rates were used according to the columns maximum pressure limit and the gradient time adjusted to keep $S{\cdot}\beta{\cdot}t_0 = 2$ constant. The figure legend provides the column brand name, pore size, total particle diameter, in brackets the shell thickness and the label L2 and L5 represent the column length of 20 and 50 mm, respectively.

ethylene hybrid (BEH) technology. Usually proteins are analysed at low pH-values but there might be some special applications where a high pH-value could provide some orthogonal selectivity or might be more beneficial for proteins with low isoelectric point. For the latter higher pH-value could enable the use of negative ionisation mode in ESI-MS-analysis [30,31]. Further, to column stability is expected to be better and it offers the possibility to use high pH for column regeneration. All tested FPP columns can be used at elevated temperatures up to 90 °C while the MAbPac column tolerates even 110 °C. This is beneficial in terms of better recovery, lower back pressure due to reduced mobile phase viscosity shifting the KPL curves to increased efficiencies and higher peak capacities, respectively. One particular disadvantage of the MAbPac column is its limited maximal pressure (275 bar) that is a result of the wide pores with limited pressure stability. It could therefore only be used at lower maximum flow rates (0.5 vs. 1.5 mL/min for most of the other tested columns) and had consequently higher retention times. Moreover, the rescaling factor λ at lower flow rates was smaller than for columns with higher pressure limits. On the other hand, the MAbPac column offers the broadest pH range (from 1 to 14) of all columns because of its polymeric support. Consequently, it can provide different selectivities because the stationary phase is based on pendant phenyl groups (divinylbenzene copolymer). The two Solas columns, however, showed their best performance for cytochrome c and lysozyme amongst the different proteins (Fig. S 6c-d). Compared to the other FPP columns, they exhibited reasonable kinetic performance for these small proteins. For the larger proteins (NISTmAb and fragments) the 400 Å Solas column is not competitive in terms of kinetic performance with the Acquity UPLC BEH C4 column, for the NISTmAb the same is seen for the 1000 Å Solas column unexpectedly. At this point it should be mentioned that both Solas columns are specified with a column maximal pressure of 700 bar, but especially the column with the 1000 Å wide pores may have limited column longevity

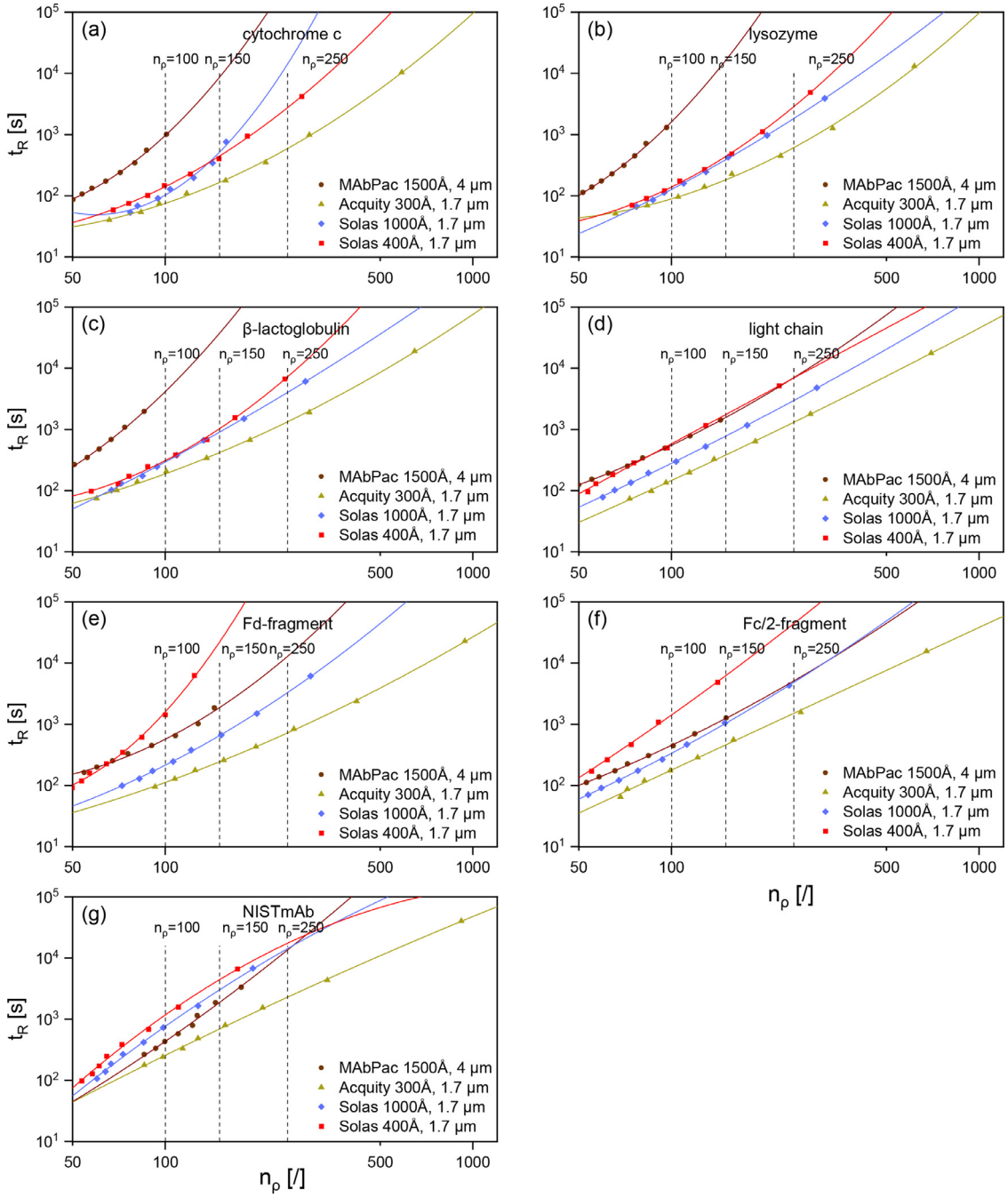

Fig. 4. Gradient kinetic plots for the same protein and different fully porous particle columns. (a) Cytochrome c, (b) lysozyme, (c) β-lactoglobulin, (d) light chain, (e) Fd-fragment, (f) Fc/2-fragment, (g) NIST mAb. Other conditions are the same as in Fig. 3. The figure legend provides the column brand name, pore size and total particle diameter.

if it is operated for prolonged period at this maximal pressure. The same trends are observed when a constant pressure limit of 700 bar is used instead of the individual column pressure limits (see supplementary Fig. S 7). Overall, the Acquity UPLC BEH C4 column showed the best kinetic performance within this class of columns regardless of protein size.

3.4. Evaluation of monolithic columns

Three monolithic columns, which differed in macropore size (and hence in domain size as well i.e. the combined length scale of mean macropore and silica skeleton diameters), mesopore size of the silica skeleton (300 and 150 Å), column dimension (4.6 and 2 mm I.D.) and alkyl-bonding (C18 vs C4), were investigated in the current study (Table 3). Of those monoliths, only the Chromolith WP300 RP-4 is dedicated for protein separations, while the Chromolith WP300 RP-18 has its application scope for larger peptides. The Chromolith HR RP-18e has its primary scope of application for small molecules and small peptides. In spite of that all three Chromoliths were investigated here for protein separations due to lack of alternatives of its kind and to illustrate performance differences that are associated with their altered morphologies, i.e. pore size, macropore and skeleton diameter that are correlated (narrower macropores are associated with thinner skeletons and smaller domain size). Hormann et al. determined macropore diameters of 1.98 ± 0.76 vs 1.33 ± 0.48 µm, skeleton diameters of 1.17 ± 0.32 vs

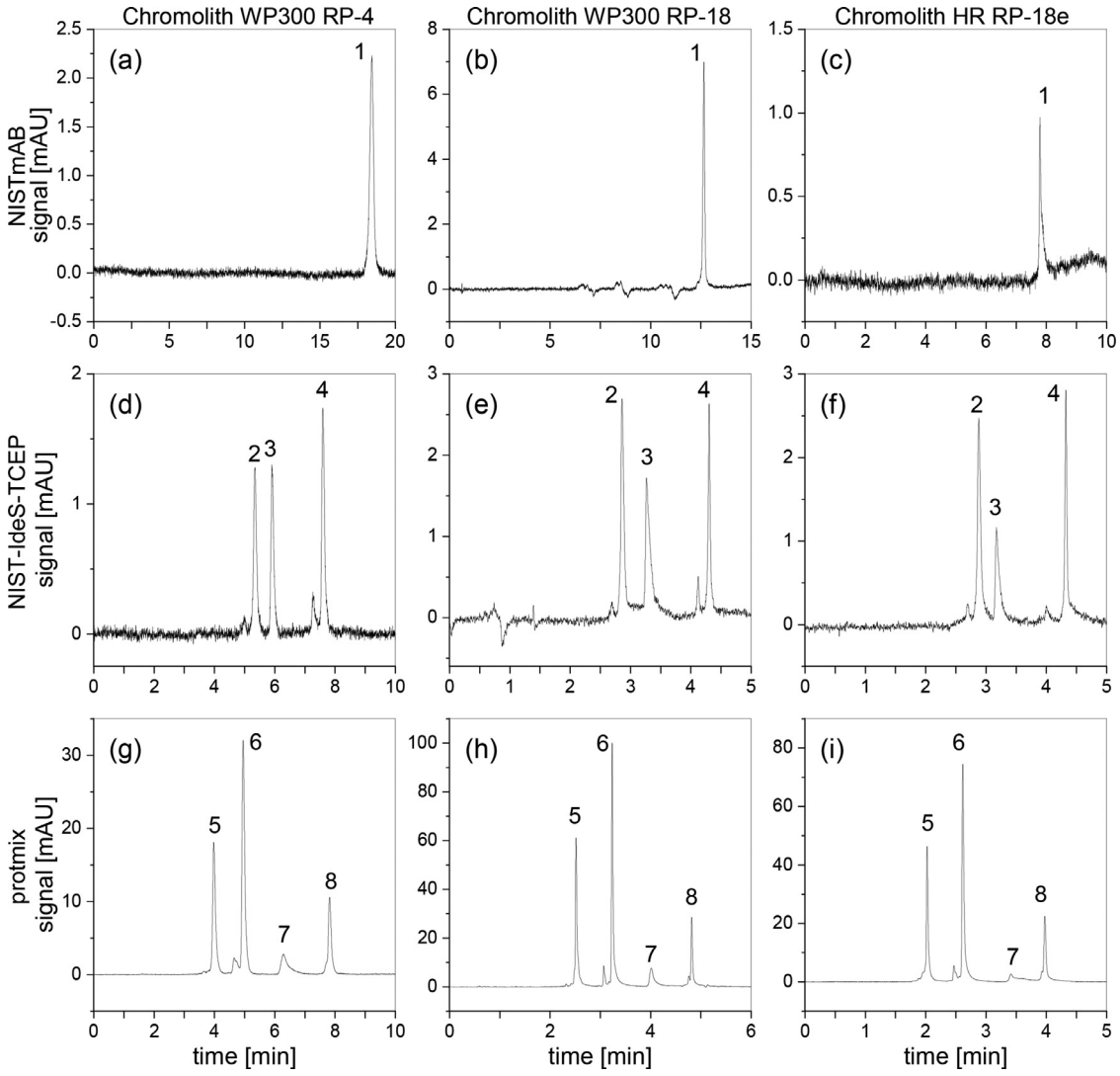

Fig. 5. Chromatogram comparison of the monolithic columns. (a-c) NISTmAb (1), (d-f) NIST-IdeS-TCEP with (2) Fc/2-, (3) light chain- and (4) Fd-fragment and protmix (g-i) containing (5) cytochrome c, (6) lysozyme, (7) BSA and (8) β-lactoglobulin. (a, d, g) Chromolith WP300 RP-4, (b, e, h) Chromolith WP 300 RP-18 and (c, f, i) Chromolith HR RP-18e columns. Column temperature = 60 °C, flow rate = 0.5 mL/min, mobile phase A: 0.1% (v/v) TFA in water, B: 0.1% (v/v) TFA in ACN, gradient 25–55% B. Gradient time was set for each column and sample mixture to keep $S{\cdot}\beta{\cdot}t_0 = 2$.

0.90 ± 0.29 µm and domain size of 3.15 vs 2.23 µm for 1st and 2nd (HR) generation of 4.6 mm I.D. Chromolith columns [32]. These dimensions are slightly downscaled for the 2 mm I.D. Chromolith columns (Table 3).

All three columns showed a good performance and could separate the two test mixtures with three sample constituents with the same elution order and similar selectivities (Fig. 5). The Chromolith WP300 RP-18 had the best performing KPL-curves for the small standard proteins cytochrome c, lysozyme and β-lactoglobulin (Fig. 6a-c). For the separation of the NISTmAb light chain and the Fd-fragment, the best kinetic performance at high flow rates (i.e. at the fast separation regime with low t_R) exhibited the Chromolith WP300 RP-18, while the Chromolith HR RP-18e performed better at lower flow rates (high peak capacity regime corresponding to the slow separation speeds see Fig. 6d-e). The Chromolith HR RP-18e is not tailored for large size proteins, but small molecule separations. Its better kinetic performance in the slow separation regime may originate from a thinner skeleton size and smaller domain size, respectively, compared to the two wide-pore monoliths, which results in lower mass transfer resistance. In the fast separation regime this advantage gets lost and the wide pore monoliths behave better and are certainly advantageous. The two C18 monoliths had a very similar performance for the Fc/2-fragment as solute (Fig. 6f).

The findings from the KPL curves for the intact NISTmAb sample were unexpected, challenging to interpret and might be easily misleading. The KPL curves shown in Fig. 6g pretend the best kinetic performance for the Chromolith HR RP-18e, especially in the slow separation speed regime. However, a low recovery was observed for this monolith which is not surprising and might be related to the hydrophobic C18 alkyl chemistry and problems in diffusional mass transfer in the narrow mesopores or even pore exclusion and blockage accompanied by analyte loss. With a hydrodynamic diameter of about 9 nm for the NISTmAb and 15 nm pore diameter, yielding a ratio $\lambda_m \sim 0.6$, effective diffusion is estimated to be significantly less than 10 % of unhindered diffusion in free solution which may partly explain the recovery loss [10]. A similar problem, however, was also found for the Chromolith WP300 RP-18 which may indicate that also the C18 surface chemistry and possibly residual silanols contribute to this poor recovery as well. The recovery was becoming worse with an increase in flow rate especially for the intact NISTmAb and the two C18 monoliths while

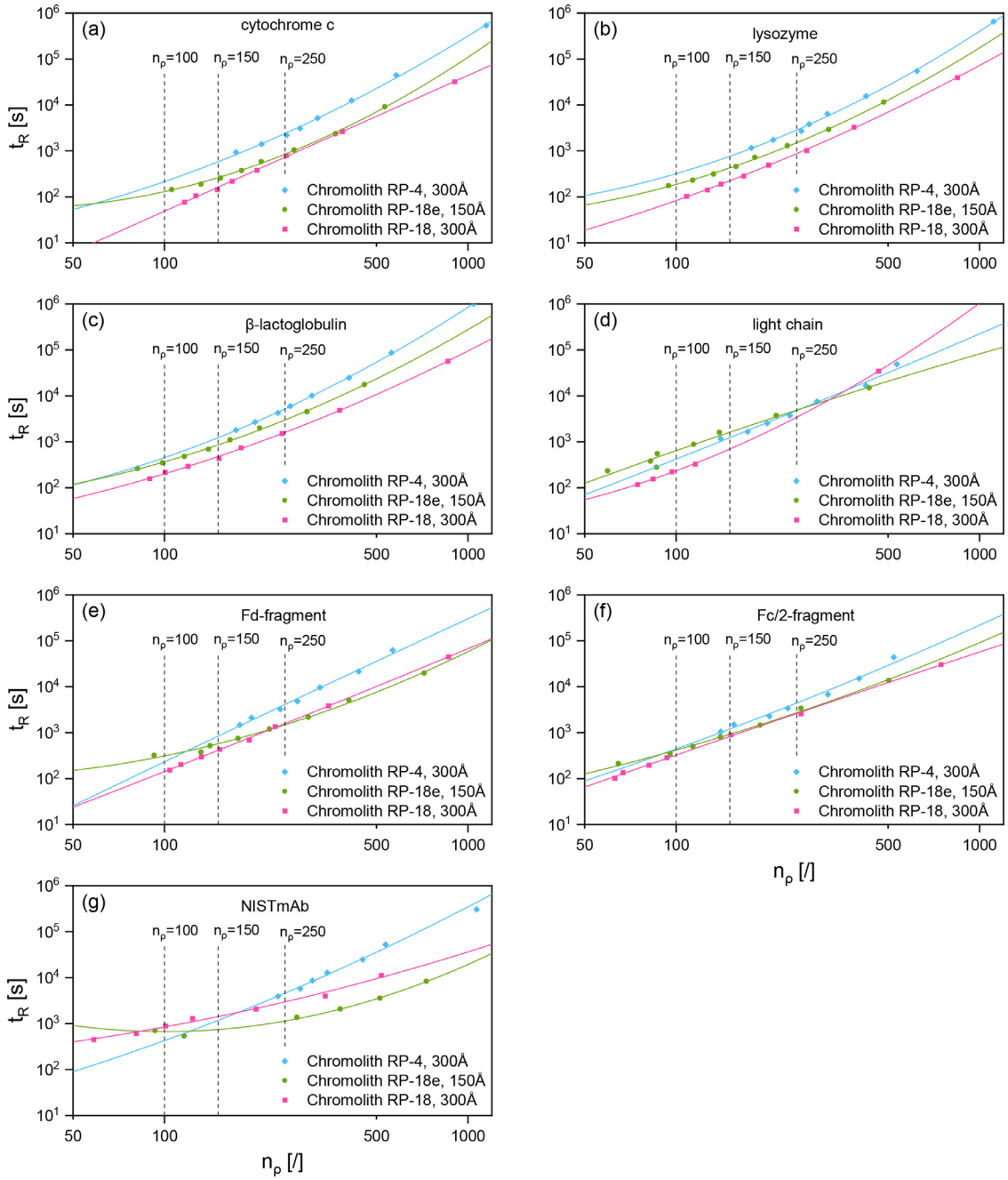

Fig. 6. Gradient kinetic plots for the same protein and different monolithic columns. (a) Cytochrome c, (b) lysozyme, (c) β-lactoglobulin, (d) light chain, (e) Fd-fragment, (f) Fc/2-fragment, (g) NIST mAb. Other conditions are the same as in Fig. 3. The figure legend provides the column brand name, stationary phase chemistry and pore size.

the C4 monolith was less affected (Fig. S 8). The recovery issue was much less problematic for the antibody fragments and the small standard proteins (Fig. S 9–10). Hence, the 300 Å wide-pore, C4 monolith column is the preferred choice, in particular for larger proteins. All protein samples had a similar KPL-curve for the Chromolith WP300 RP-4 column (Fig S 11).

3.5. Comparison of column technologies

KPL curves have the advantage that they enable a reasonable direct comparison of columns with different dimensions and stationary phase morphologies. Hence, such kinetic plots are a good approach to figure out which column provides the best performance across distinct morphologies for a given application. For this purpose, a comparison of the columns from all designs was finally carried out. The chromatograms of the best performing column from each column technology at the same flow rate are depicted in Fig. 2. The KPL-curves from the best and least performing column of each column technology are shown in (Fig. 7a-g). A detailed discussion focused on the pore size influence of a representative pair of columns from each column morphology is furthermore provided in the supplementary information (chapter 2.7 and Fig. S 12).

The best columns for SPP, FPP and monolith technology were the BIOshell 400 Å, Acquity UHPLC protein BEH C4 and Chromolith WP300 RP-18 columns, respectively. Across all protein sizes, except for NISTmAb the BIOshell 400 Å column showed the best kinetic performance. It was outperformed, though, by the Acquity UHPLC protein BEH C4 and Chromolith WP300 RP-18 columns in

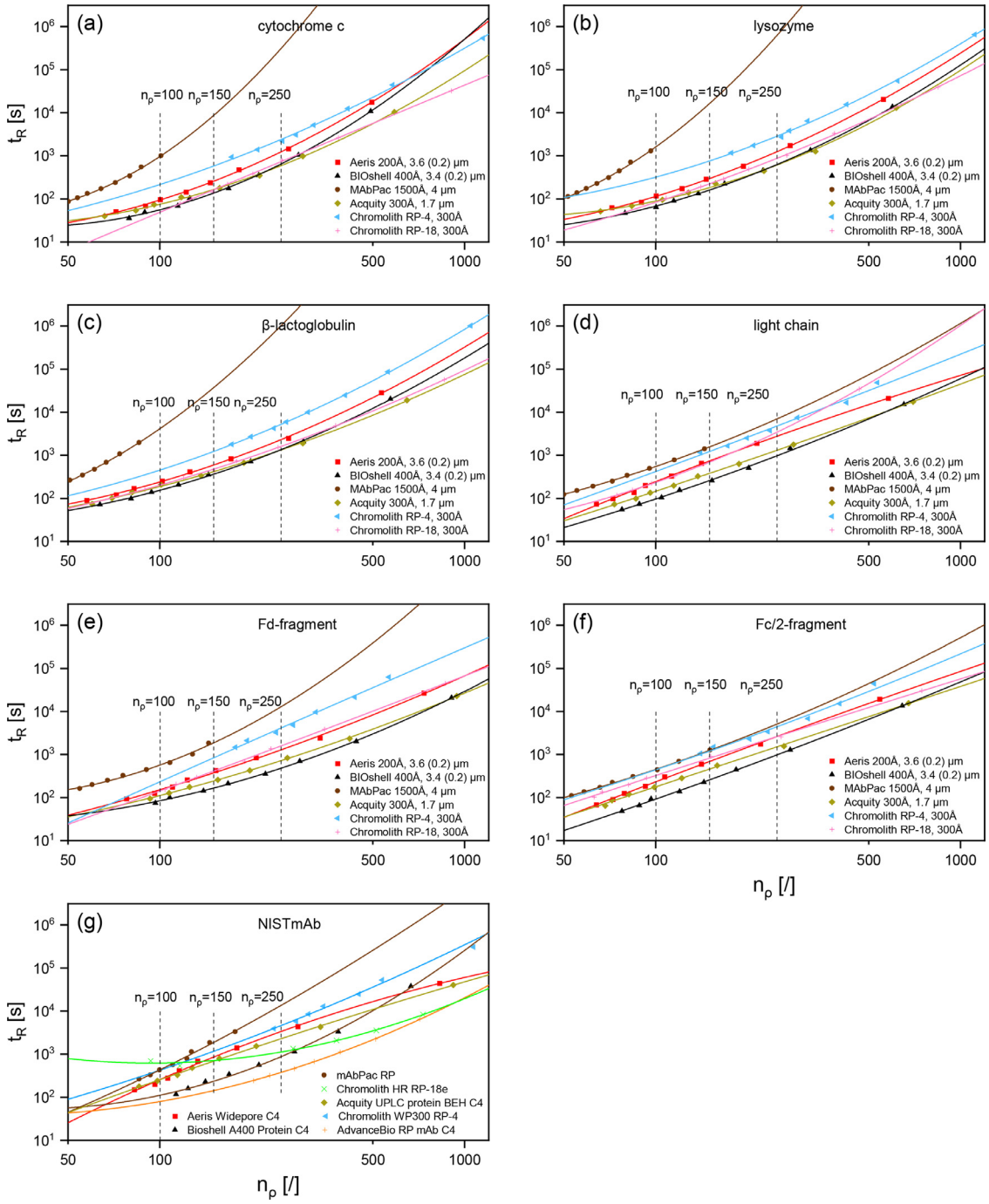

Fig. 7. Gradient kinetic plot comparison of best and worst column for each column technology and a certain protein. Other conditions are the same as in Fig. 3. The figure legend provides the column brand name, pore size, total particle diameter, in brackets the shell thickness and the label L2 and L5 represent the column length of 20 and 50 mm, respectively.

the low speed region for the small proteins. The Acquity UHPLC protein BEH C4 column showed comparable performance for the small proteins but fell short, compared to BIOshell 400 Å, for the larger protein sizes. Even the SPP with the lowest performance, the Aeris Widepore C4 column, showed only a little worse performance and was still a good candidate for the separation of small proteins. The MAbPac RP column was clearly less favourable in terms of kinetic performance, yet since the 1500 Å pores are fully accessible even for larger proteins it may offer favourable interactive surface and selectivity depending on the protein mixture. The KPL-curves for the intact NISTmAb were considerably different compared to all smaller protein samples (Fig. 7g). The SPP AdvanceBIO RP mAb C4 had clearly the best performance, followed by the BIOshell 400 Å. The KPL-curve of the Aeris Widepore C4 (200 Å) largely matched the one of FPP Acquity UHPLC BEH protein C4 (300 Å). The shorter diffusion paths of the former might compensate for the favourable wider pores of the latter. As expected, the pore size of the Chromolith HR RP-18e is too small for protein separations resulting in recovery problems (vide supra). On the other hand, the Chromolith WP300 RP-18 was quite competitive to the best performing columns Acquity UHPLC BEH C4 (FPP) and BIOshell 400 Å (SPP) for the small proteins. For large

proteins like mAbs the Chromolith WP300 RP-4 is the preferred choice and its KPL approximate the SPP (Aeris Widepore C4) and FPP columns (Acquity UHPLC BEH protein C4) with similar pore size. Major limitations of the monoliths were their low maximum pressure drop (originating mostly due to the fragile PEEK cladding) and the large total porosity. The maximum pressure limit for the Chromolith columns was at only 200 bar which was the lowest for all the 13 columns and effected the KPL curves through the rescaling factor λ. In spite of the low pressure limit, it was still possible to use a high flow rate of 1.5 mL/min due to the low column back pressure. Overall the SPP columns (BIOshell 400 Å and AdvanceBIO RP mAb C4) showed the best performance and the FPP Acquity UHPLC BEH C4 also an excellent performance for the small proteins and antibody fragments.

4. Conclusions

Gradient kinetic plots are a powerful tool for the evaluation of the column performance and can be conveniently applied even when they have distinct stationary phase morphologies. The current work provides an extended performance evaluation of new and relatively established modern columns for the separation of proteins. For that purpose, a set of proteins was used to cover a molecular weight range from 12.4 to 148 kDa and consisted of standard proteins (cytochrome c, lysozyme and β-lactoglobulin), an intact monoclonal antibody (NISTmAb) and its fragments after IdeS-digestion and disulphide reduction. Superficially porous particle (SPP) columns, in particular with thin shell, showed overall the best performance among all the tested columns due to their outstanding mass transfer kinetics in combination with the possibility to be used at ultra-high pressure. This enables their usage for ultra-fast separations what is a continuous demand from the (pharmaceutical) industry and important for full comprehensive two-dimensional liquid chromatography. In the fast separation regime, a thinner porous shell was outperforming wider pore size. A sub-2 µm fully porous particle (FPP) column and monolithic columns could compete with the superficially porous columns for small sized proteins but were clearly outperformed by the SPP column with thin shell for the analysis of the antibody and its fragments. Mass transfer resistance has the biggest contribution to band broadening especially at high flow rates, therefore, the diffusion path lengths must be reduced by using thin porous shell for SPP columns and reducing the particle size for FPPs. The pore size has a critical influence on the mass transfer kinetics and a value of around 400 Å seems to be optimal for a broad range of protein sizes but larger pore can be more beneficial if the diffusion path is longer. Monolithic columns benefit from a low column back pressure but due to their lower pressure stability they can be damaged more easily by ultra-high pressure systems. However, the selection of columns for protein separations should not solely be based on the kinetic performance but should also consider factors like protein recovery (adsorption), selectivity, silanol activity and temperature stability to mention a few. Overall, the current study may guide column selection for specific protein sizes.

Declaration of Competing Interest

The authors declared no conflicts of interest.

CRediT authorship contribution statement

Simon Jaag: Investigation, Methodology, Formal analysis, Visualization, Writing – original draft. **Chunmei Wen:** Investigation, Formal analysis, Visualization, Methodology, Writing – review & editing. **Benjamin Peters:** Methodology, Data curation, Writing – review & editing. **Michael Lämmerhofer:** Conceptualization, Methodology, Supervision, Writing – review & editing, Resources.

Acknowledgements

We thank Benjamin Peters from Merck KGaA, Darmstadt, Germany for generous gift of research samples of Chromolith columns.

Supplementary materials

Supplementary material associated with this article can be found, in the online version, at doi:10.1016/j.chroma.2022.463251.

References

[1] C. Morrison, Fresh from the biotech pipeline—2019, Nat. Biotechnol. 38 (2) (2020) 126–131, doi:10.1038/s41587-019-0405-7.
[2] G. Walsh, Biopharmaceutical benchmarks 2018, Nat. Biotechnol. 36 (12) (2018) 1136–1145, doi:10.1038/nbt.4305.
[3] A. Beck, E. Wagner-Rousset, D. Ayoub, A. Van Dorsselaer, S. Sanglier-Cianférani, Characterization of therapeutic antibodies and related products, Anal. Chem. 85 (2) (2013) 715–736, doi:10.1021/ac3032355.
[4] S. Fekete, A. Murisier, A. Beck, J. Lawhorn, H. Ritchie, B. Boyes, D. Guillarme, New wide-pore superficially porous stationary phases with low hydrophobicity applied for the analysis of monoclonal antibodies, J. Chromatogr. A 1642 (2021) 462050, doi:10.1016/j.chroma.2021.462050.
[5] D.V. McCalley, D. Guillarme, Evaluation of additives on reversed-phase chromatography of monoclonal antibodies using a 1000 Å stationary phase, J. Chromatogr. A (2019) 460562, doi:10.1016/j.chroma.2019.460562.
[6] S. Fekete, S. Rudaz, J.-L. Veuthey, D. Guillarme, Impact of mobile phase temperature on recovery and stability of monoclonal antibodies using recent reversed-phase stationary phases, J. Sep. Sci. 35 (22) (2012) 3113–3123, doi:10.1002/jssc.201200297.
[7] M.C. Garcıá, A.C. Hogenboom, H. Zappey, H. Irth, Effect of the mobile phase composition on the separation and detection of intact proteins by reversed-phase liquid chromatography–electrospray mass spectrometry, J. Chromatogr. A 957 (2) (2002) 187–199 https://doi.org/10.1016/S0021-9673(02)00345-X.
[8] S. Fekete, B. Bobály, J.M. Nguyen, A. Beck, J.-L. Veuthey, K. Wyndham, M.A. Lauber, D. Guillarme, Use of ultrashort columns for therapeutic protein separations. Part 1: theoretical considerations and proof of concept, Anal. Chem. 93 (3) (2021) 1277–1284, doi:10.1021/acs.analchem.0c04082.
[9] L.R. Snyder, M.A. Stadalius, M.A. Quarry, Gradient elution in reversed-phase HPLC-separation of macromolecules, Anal. Chem. 55 (14) (1983) 1412A–1430A, doi:10.1021/ac00264a001.
[10] B.M. Wagner, S.A. Schuster, B.E. Boyes, T.J. Shields, W.L. Miles, M.J. Haynes, R.E. Moran, J.J. Kirkland, M.R. Schure, Superficially porous particles with 1000 Å pores for large biomolecule high performance liquid chromatography and polymer size exclusion chromatography, J. Chromatogr. A 1489 (2017) 75–85, doi:10.1016/j.chroma.2017.01.082.
[11] W. Chen, K. Jiang, A. Mack, B. Sachok, X. Zhu, W.E. Barber, X. Wang, Synthesis and optimization of wide pore superficially porous particles by a one-step coating process for separation of proteins and monoclonal antibodies, J. Chromatogr. A 1414 (2015) 147–157, doi:10.1016/j.chroma.2015.08.043.
[12] S.A. Schuster, B.M. Wagner, B.E. Boyes, J.J. Kirkland, Optimized superficially porous particles for protein separations, J. Chromatogr. A 1315 (2013) 118–126, doi:10.1016/j.chroma.2013.09.054.
[13] D. Stoll, S. Fekete, D. Guillarme, Tips, tricks, and troubleshooting for separations of biomolecules, part i: contemporary reversed-phase protein separations, LCGC North Am. 36 (7) (2018) 440–446.
[14] K. Horváth, F. Gritti, J.N. Fairchild, G. Guiochon, On the optimization of the shell thickness of superficially porous particles, J. Chromatogr. A 1217 (41) (2010) 6373–6381, doi:10.1016/j.chroma.2010.08.013.
[15] J.L. Dores-Sousa, A. Fernández-Pumarega, J. De Vos, M. Lämmerhofer, G. Desmet, S. Eeltink, Guidelines for tuning the macropore structure of monolithic columns for high-performance liquid chromatography, J. Sep. Sci. 42 (2) (2019) 522–533, doi:10.1002/jssc.201801092.
[16] D. Cabooter, K. Broeckhoven, R. Sterken, A. Vanmessen, I. Vandendael, K. Nakanishi, S. Deridder, G. Desmet, Detailed characterization of the kinetic performance of first and second generation silica monolithic columns for reversed-phase chromatography separations, J. Chromatogr. A 1325 (2014) 72–82, doi:10.1016/j.chroma.2013.11.047.
[17] J.L. Dores-Sousa, J. De Vos, S. Eeltink, Resolving power in liquid chromatography: a trade-off between efficiency and analysis time, J. Sep. Sci. 42 (1) (2019) 38–50, doi:10.1002/jssc.201800891.
[18] T.J. Causon, K. Broeckhoven, E.F. Hilder, R.A. Shellie, G. Desmet, S. Eeltink, Kinetic performance optimisation for liquid chromatography: Principles and practice, J. Sep. Sci. 34 (8) (2011) 877–887, doi:10.1002/jssc.201000904.
[19] G. Desmet, D. Cabooter, K. Broeckhoven, Graphical data representation methods to assess the quality of LC columns, Anal. Chem. 87 (17) (2015) 8593–8602, doi:10.1021/ac504473p.

[20] K. Broeckhoven, D. Cabooter, F. Lynen, P. Sandra, G. Desmet, The kinetic plot method applied to gradient chromatography: theoretical framework and experimental validation, J. Chromatogr. A 1217 (17) (2010) 2787–2795, doi:10.1016/j.chroma.2010.02.023.
[21] S. Fekete, R. Berky, J. Fekete, J.-L. Veuthey, D. Guillarme, Evaluation of a new wide pore core–shell material (Aeris™ WIDEPORE) and comparison with other existing stationary phases for the analysis of intact proteins, J. Chromatogr. A 1236 (2012) 177–188, doi:10.1016/j.chroma.2012.03.018.
[22] B. Bobály, M. Lauber, A. Beck, D. Guillarme, S. Fekete, Utility of a high coverage phenyl-bonding and wide-pore superficially porous particle for the analysis of monoclonal antibodies and related products, J. Chromatogr. A 1549 (2018) 63–76, doi:10.1016/j.chroma.2018.03.043.
[23] L. Nováková, A. Vaast, C. Stassen, K. Broeckhoven, M. De Pra, R. Swart, G. Desmet, S. Eeltink, High-resolution peptide separations using nano-LC at ultra-high pressure, J. Sep. Sci. 36 (7) (2013) 1192–1199, doi:10.1002/jssc.201201087.
[24] A. Vaast, K. Broeckhoven, S. Dolman, G. Desmet, S. Eeltink, Comparison of the gradient kinetic performance of silica monolithic capillary columns with columns packed with 3 μm porous and 2.7 μm fused-core silica particles, J. Chromatogr. A 1228 (2012) 270–275, doi:10.1016/j.chroma.2011.07.089.
[25] T. Hetzel, C. Blaesing, M. Jaeger, T. Teutenberg, T.C. Schmidt, Characterization of peak capacity of microbore liquid chromatography columns using gradient kinetic plots, J. Chromatogr. A 1485 (2017) 62–69, doi:10.1016/j.chroma.2017.01.018.
[26] J.W. Thompson, T.J. Kaiser, J.W. Jorgenson, Viscosity measurements of methanol–water and acetonitrile–water mixtures at pressures up to 3500 bar using a novel capillary time-of-flight viscometer, J. Chromatogr. A 1134 (1) (2006) 201–209, doi:10.1016/j.chroma.2006.09.006.
[27] Y. Zhang, X. Wang, P. Mukherjee, P. Petersson, Critical comparison of performances of superficially porous particles and sub-2 μm particles under optimized ultra-high pressure conditions, J. Chromatogr. A 1216 (21) (2009) 4597–4605, doi:10.1016/j.chroma.2009.03.071.
[28] M. Gilar, U.D. Neue, Peak capacity in gradient reversed-phase liquid chromatography of biopolymers: theoretical and practical implications for the separation of oligonucleotides, J. Chromatogr. A 1169 (1) (2007) 139–150, doi:10.1016/j.chroma.2007.09.005.
[29] S. Jaag, M. Shirokikh, M. Lämmerhofer, Charge variant analysis of protein-based biopharmaceuticals using two-dimensional liquid chromatography hyphenated to mass spectrometry, J. Chromatogr. A 1636 (2021) 461786, doi:10.1016/j.chrom.2020.461786.
[30] L. Konermann, D.J. Douglas, Unfolding of proteins monitored by electrospray ionization mass spectrometry: a comparison of positive and negative ion modes, J. Am. Soc. Mass. Spectrom. 9 (12) (1998) 1248–1254 https://doi.org/10.1016/S1044-0305(98)00103-2.
[31] I. Liko, J.T.S. Hopper, T.M. Allison, J.L.P. Benesch, C.V. Robinson, Negative ions enhance survival of membrane protein complexes, J. Am. Soc. Mass. Spectrom. 27 (6) (2016) 1099–1104, doi:10.1007/s13361-016-1381-5.
[32] K. Hormann, T. Müllner, S. Bruns, A. Höltzel, U. Tallarek, Morphology and separation efficiency of a new generation of analytical silica monoliths, J. Chromatogr. A 1222 (2012) 46–58, doi:10.1016/j.chroma.2011.12.008.